Eur. Phys. J. A (2017) **53**: 46
DOI 10.1140/epja/i2017-12231-8

THE EUROPEAN PHYSICAL JOURNAL A

Regular Article – Experimental Physics

Thermal neutron capture cross-section and resonance integral measurements of ^{139}La(n, γ)^{140}La and ^{140}Ce(n, γ)^{141}Ce using a Am-Be neutron source

Priyada Panikkath[a] and P. Mohanakrishnan

Manipal Centre for Natural Sciences, Manipal University, Karnataka-576104, India

Received: 13 December 2016 / Revised: 31 January 2017
Published online: 8 March 2017 –
Communicated by R.K. Bhandari

Abstract. Thermal neutron capture cross-sections and resonance integrals of ^{139}La(n, γ)^{140}La and ^{140}Ce (n, γ)^{141}Ce are measured with respect to reference reactions ^{197}Au(n, γ)^{198}Au and ^{55}Mn(n, γ)^{56}Mn using the neutron activation technique. Measurements are carried out using neutrons from an Am-Be source located inside a concrete bunker. Two different methods are used for determining self-shielding factors of activation foils as well as for finding the epithermal neutron spectrum shape factor. For ^{139}La with reference to ^{197}Au and ^{55}Mn the measured thermal cross sections are 9.24 ± 0.25 b and 9.28 ± 0.37 b, respectively, while the measured resonance integrals are 12.18 ± 0.67 b and 11.81 ± 0.94 b, respectively. For ^{140}Ce with reference to ^{197}Au and ^{55}Mn the measured thermal cross sections are 0.44 ± 0.01 b and 0.44 ± 0.02 b, respectively, while the measured resonance integrals are 0.55 ± 0.03 b and 0.54 ± 0.04 b, respectively. The present measurements are compared with earlier measurements and evaluations. Presently estimated values confirm the established ^{139}La(n, γ)^{140}La cross-sections. The presently measured thermal capture cross-section ^{140}Ce(n, γ)^{141}Ce, though lower than the evaluated data, is having higher accuracy compared to previous measurements with large uncertainties. The resonance integral measured is higher (like most previous measurements) than most evaluations requiring a revision of the evaluated data.

1 Introduction

Neutron-induced reaction cross-section measurements are of great importance to the nuclear technology. Advanced nuclear technologies like Accelerator Driven Subcritical systems (ADS), Th-U fuel cycles and fusion reactors etc. require large refinement and new measurements of neutron cross section data of structural materials, nuclear fuels and the fission products. The nuclear reactor design, shielding design, build-up and decay heat estimation, nuclear waste and transmutation studies etc. rely crucially on the evaluated nuclear data. The spread among different cross-section measurements is still found to be large [1] compared to the requirement (uncertainty $\leq 5\%$) for various applications. The need for such measurements and theoretical studies are emphasised in one of the review articles [2]. Thermal neutron capture cross-sections and the resonance integrals can be measured using the neutron activation technique, where the neutron source can be a reactor beam, a D-T accelerator beam or even an isotopic source like Am-Be as has been done recently for isotopes ^{138}Ba and ^{141}Pr [3].

The isotopes ^{139}La and ^{140}Ce are important fission products in the fuel cycle of the thermal neutron-induced fission of ^{233}U and ^{235}U and fast neutron-induced fission of ^{239}Pu. ^{139}La is one of the important fission products that forms from the decay chain ^{139}Xe-^{139}Cs-^{139}Ba-^{139}La other than its direct yield from fission. ^{140}Ce is also produced in significant quantities from the decay chain of ^{140}Xe-^{140}Cs-^{140}Ba-^{140}La-^{140}Ce as well as directly from fission. The neutron capture of ^{139}La is used to measure the operating power distribution by activation gamma measurements after the reactor shutdown. The activity of ^{140}La produced on the neutron capture of ^{139}La is analyzed routinely in test reactors and correlates the results with the ^{137}Cs results [4]. The sufficiently high gamma energy, gamma yield and short half-life of ^{140}La makes it an ideal radiotracer in many industrial applications. The cumulative yields of ^{139}La and ^{140}Ce are greater than 6% in the thermal neutron-induced fission of ^{233}U/^{235}U and are greater than 5% in the fast neutron-induced fission of ^{239}Pu [5]. Thus, the neutron capture cross-sections of ^{139}La and ^{140}Ce either as integrals or as point data are important in nuclear reactor fuel related calculations.

After a careful literature survey with the help of EXFOR database [6], the present status of measured or

[a] e-mail: priyada.p@manipal.edu

evaluated thermal neutron capture cross-sections and resonance integrals of the above two isotopes are compiled. The thermal neutron capture cross-section and the resonance integral of ^{139}La(n, γ)^{140}La are well studied using the activation technique. As per the EXFOR compilations, there are 13 thermal neutron capture cross-section [7–18] and resonance integral measurements each [7, 12, 19–28]. The various evaluated data are compiled for comparison [5, 29–35]. The measured thermal neutron capture cross-sections vary between 8.1 b and 9.5 b and the evaluated thermal neutron capture cross-sections are either 8.94 b or 9.04 b. However, there is a wide spread in the measured resonance integral of ^{139}La between 7.5 b and 12.6 b while the evaluated resonance integral are between 11.45 b and 12.10 b. There are seven measured thermal neutron capture cross-sections and resonance integrals of ^{140}Ce(n,)^{141}Ce [20, 22–24, 36–41]. The measured thermal neutron capture cross-section and resonance integral data are spread between 0.24 b–0.68 b and 0.43 b–0.66 b, respectively. Thus the spread in the measured thermal neutron capture cross-section is high as against the evaluations [5, 29–35] which are in good agreement with each other (0.57 b–0.58 b). However, the resonance integrals reported by various evaluations are not in good agreement and vary between 0.28 b and 0.54 b. Also the measurements suggest a higher value. The above observations suggest the requirement of more accurate measurements and evaluations especially in the case of ^{140}Ce.

The present study focuses on the measurement of the thermal neutron capture cross-sections and the resonance integrals of ^{139}La and ^{140}Ce using an Am-Be neutron source placed inside a concrete bunker with reference to ^{197}Au(n, γ)^{198}Au and ^{55}Mn(n, γ) ^{56}Mn reactions. ^{197}Au is one of the widely used reference monitors in the neutron activation technique. There are few measurements available in the literature where ^{55}Mn is used as reference monitor [42]. The feasibility of using an high intense Am-Be neutron source kept inside a concrete bunker for the thermal neutron capture cross-section and the resonance integral measurement has been established in our previous work [3]. Further, the uncertainty of measured cross-sections in this study is lower (about 2%–8%) as compared to the previous work where it was about 5%–12%. The low neutron flux of such a neutron source compared to the reactor neutrons is offset partly by increasing the sample weight. In addition, irradiation till the activity saturation is also followed wherever possible. The details about the experimental set-up, procedure followed and data analysis are explained in the subsequent sections.

2 Experimental methods

The Am-Be neutron source, available at the neutron physics laboratory of Manipal Centre for Natural Science, Manipal University, has a yield of 4×10^7 neutrons/second in 4π geometry. The source is kept inside a concrete bunker with an opening in one of the sides for facilitating the irradiation of the samples. The experimental geometry is similar to the one reported in the previous work [3]. The

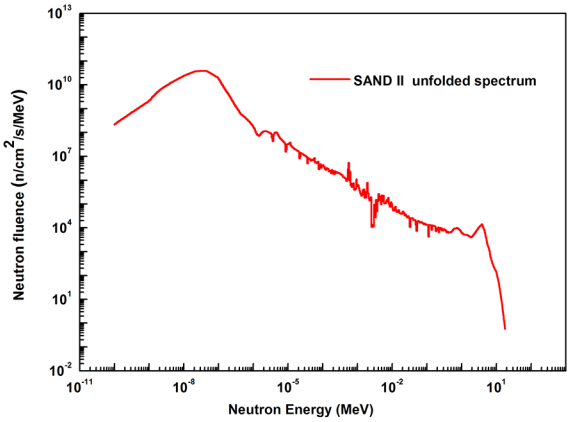

Fig. 1. The neutron spectra at the irradiation location unfolded using the SAND-II code by the multiple foil activation technique [3].

neutron spectrum from an Am-Be source gets moderated due to the multiple scattering in this surrounding concrete structure. Thus, the neutron spectrum has a mixed component including the thermal ($E < 0.55$ eV), epithermal (0.55 eV $< E <$ 100 keV) and fast ($E >$ 100 keV) ones. The neutron spectra at various locations inside the experimental channel are simulated using a Monte Carlo simulation by incorporating the exact experimental geometry. Additionally, the neutron spectra are characterized by the multi-foil activation technique using the activation foils of Au, In, Mn, Sc, Cu, Mo, Na, Fe, Ni and Al. The measured reaction rates are used to unfold the neutron spectrum using the SAND-II code [43]. It may be mentioned that Mo activation cross-sections were newly generated from the Reference Neutron Activation Library [44] and added to SAND-II cross-section data at our centre. In the SAND-II code, the reaction rates are estimated using the guess spectrum and compares with the measured values. The guess spectrum is further adjusted and the process repeats till the required accuracy or convergence is obtained. In the present case, the iteration continued till convergence and the standard deviation between the measured reaction rates and the calculated reaction rates is 3.68%. The unfolded spectra has a dependence on the *a priori* guess spectrum and in the present study the simulated neutron spectra using Monte Carlo code MCNP [45] are used as initial guess spectra. The SAND-II unfolded spectrum at the irradiation location is shown in fig. 1 [3]. The total neutron fluence obtained from both simulation (5.7×10^4 n/cm^2/s) and the SAND-II unfolding (5.39×10^4 n/cm^2/s) are in good agreement. At the irradiation location, the thermal neutron fluence and the epithermal neutron fluence are estimated as (5×10^3 n/cm^2/s) and (7×10^3 n/cm^2/s), respectively.

Activation foils of Mn (Mn(83%)-Cu) and Au having 12 mm diameter procured from Shieldwerx with purity 99.9% were used as reference isotopes. Analytical grade powder samples of La_2O_3 and Ce_2O procured from Star Rare Earth Ltd were used for the measurements. The weight of each samples is shown in table 1. Two sets of

Table 1. Nuclear decay data (gamma energy (E_γ), gamma yield (I_γ) and the half-life ($T_{1/2}$) [46], effective resonance energy (Er) [48], gamma attenuation factor (f) and the Westcott factor (g) [34]) of the samples used in the calculations.

Target	Foil/Sample	Weight (mg)	E_γ (keV)	I_γ (%)	$T_{1/2}$	Er (eV)	f	g
^{197}Au	Au	125 ± 0.6	411.8	95.54 ± 0.07	2.6944 ± 0.0008 d	5.47	1.009	1.0054
^{55}Mn	Mn(83%)-Cu	40 ± 0.2	846.7	98.85 ± 0.03	2.57878 ± 0.00046 h	468	1.005	1.0003
^{139}La	La_2O_3	511 ± 11	1596.2	95.4 ± 0.08	1.67850 ± 0.00017 d	76	1	0.9996
^{140}Ce	CeO_2	1000 ± 2	145.5	48.29 ± 0.19	32.503 ± 0.011 d	7200	1.09	1.0003

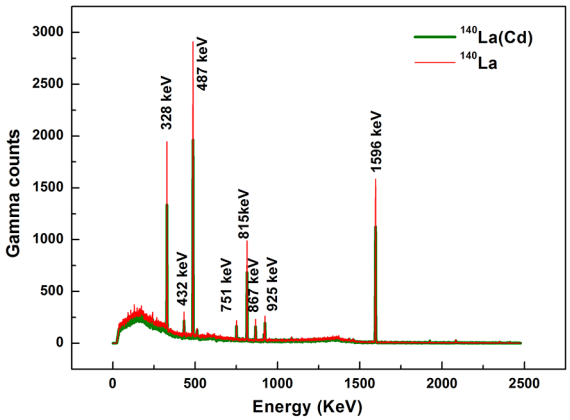

Fig. 2. Measured gamma spectra from ^{139}La sample irradiated in the neutron field with (green) and without (red) cadmium cover.

each sample were used in the experiment; one of them was irradiated by enclosing in a cadmium cover and the other without cadmium cover. Standard cadmium cover provided by Shieldwerx is used in the experiment. La sample and the reference monitors were irradiated placing together side by side for 10 days. The distance between the foils was around 10 mm such that the flux depression due to the presence of Cd is negligible. The irradiations were repeated with another set of samples with similar dimensions for a longer duration of 15 days. Owing to the larger half-life of the ^{141}Ce sample (table 1), the Ce samples were irradiated for 32 days (one half life) along with the reference monitors. The induced activity in each of the sample after irradiation is estimated from the corresponding gamma spectra. Gamma spectrum measurements were carried out using a 30% relative efficiency HPGe detector pre-calibrated using a ^{152}Eu source. The distance between the samples and the detector was 2 cm. The possibility of co-incidence summing effect is neglected in the present study due to the lower activity produced on irradiation in comparison with the irradiation in a reactor neutron field. Each of the samples was counted for 7200 s–80000 s depending upon the half-life to achieve a satisfactory counting statistics. Figure 2 shows the gamma spectra of ^{140}La formed by the neutron capture of ^{139}La. The decreased activity for the cadmium covered sample can be clearly seen from fig. 2 for the same counting duration.

The net areas (C) under the full peaks of energies mentioned in table 1 are obtained from the background-subtracted gamma spectra. The reaction rate per target atom (R) is estimated from these net areas using the following relation:

$$R = \frac{C\lambda}{[1-e^{-\lambda t_{irr}}][e^{-\lambda t_d}][1-e^{-\lambda t_c}]} \frac{Mf}{N_A \theta \epsilon I_\gamma m}, \quad (1)$$

where λ is the decay constant in s^{-1}, t_{irr} is the irradiation duration, t_d is the delay time, t_c is the counting time, ε is efficiency of the detector, I_γ is gamma yield, N_A is the Avogadro number, θ is the isotopic abundance, f is the gamma attenuation factor, m is the weight of the target and M is the atomic mass. The correction factor, f, is determined using the energy and material-dependent linear attenuation coefficient (μ) taken from XCOM photon data base [47].

3 Formulation of thermal capture cross-section and resonance integral

The thermal-neutron capture cross-sections (σ_0) and the resonance integrals (I_0) are determined from the reaction rates measured from the induced activities of the irradiated foils using gamma spectroscopy. Reaction rates of bare (R) and cadmium covered (R_{Cd}) targets are calculated using eq. (1). The σ_0 of the sample can be estimated with respect to the reference monitor. In the present study, σ_0 of the samples are estimated with reference to the thermal capture cross-section of ^{197}Au (98.71 b) and ^{55}Mn (13.41 b) [33]:

$$\sigma_{0,S} = \frac{(R - \frac{R_{Cd}}{F_{Cd}})_S (G_{th})_{Rf}}{(R - \frac{R_{Cd}}{F_{Cd}})_{Rf} (G_{th})_S} \frac{g_{Rf}}{g_S} \sigma_{0,Rf}. \quad (2)$$

The subscripts S and Rf are indicating either the sample or the reference monitor, respectively. F_{Cd} is the cadmium transmission factor which accounts for the specific count rate difference due to the cadmium cover. The F_{Cd} value for ^{197}Au is 0.991 and for the other three isotopes considered in the present study is 1.0 [8, 48]. The deviation of the cross-section from $1/\nu$ behaviour is accounted by the Westcott factor represented as g in the equation. The resonance integral ($I_0(\alpha)$) for a real epithermal spectrum with an epithermal shaping factor, (α) can be obtained

from the measured reaction rates using the equation

$$I_0(\alpha)_S = I_0(\alpha)_{Rf} \frac{g_S}{g_{Rf}} \frac{(\sigma_{0,S})(F_{Cd}CR-1)_{Rf}}{(\sigma_{0,Rf})(F_{Cd}CR-1)_S} \times \left(\frac{G_{epi}}{G_{th}}\right)_{Rf} \left(\frac{G_{th}}{G_{epi}}\right)_S . \quad (3)$$

In eq. (3), the ratio of the reaction rates of bare and cadmium covered foils is represented by CR. The resonance integrals of ^{197}Au (1563 b) and ^{55}Mn (11.76 b) are used as the reference values [33]. $I_0(\alpha)$ is the energy and neutron spectra dependent parameter and it can be related to the ideal resonance integral I_0, as shown in eq. (4) [7]:

$$I_0(\alpha) = (1\,\text{eV})^\alpha \frac{I_0 - 0.426\sigma_0}{(Er)^\alpha} + \frac{0.426\sigma_0}{(2\alpha+1)(E_{Cd})^\alpha} , \quad (4)$$

where Er is the effective resonance energy, E_{Cd} is the cadmium cut off energy and 1 eV is the reference energy. This relation is valid for $E_{Cd} = 0.55$ eV since the value 0.426 in eq. (4) is obtained from $2\frac{E_0}{E_{Cd}}^{0.5}$, where $E_0 = 0.025$ eV.

3.1 Estimation of the epithermal spectrum shaping factor

The epithermal spectrum shaping factor denoted by α accounts the deviation of the neutron flux from $\frac{1}{E}$ dependence. The resonance integrals measured in an experimental facility can be converted to the ideal resonance integral by knowing the spectrum shaping factor of the irradiated neutron spectrum. The spectrum shaping factor can be estimated using the cadmium-covered dual monitors or the multiple monitor method [49, 50]. The reaction rates of the reference monitors Au and Mn are used to estimate the spectrum shaping factor α using the dual monitor method by equating the flux ratio using eq. (4) and eq. (5) [51]. The estimated spectrum shaping factor using the dual monitor method is found to be -0.142:

$$\left[(F_{Cd}CR-1)\frac{G_{epi}}{G_{th}}\frac{I_0(\alpha)}{g\sigma_0}\right]_{Au} = \left[(F_{Cd}CR-1)\frac{G_{epi}}{G_{th}}\frac{I_0(\alpha)}{g\sigma_0}\right]_{Mn} . \quad (5)$$

The epithermal spectrum shaping factor is also obtained by fitting the SAND-II neutron spectrum between 0.55 eV and 100 keV using a non-linear fitting function having the form $\phi(E) = A/E^{(1+\alpha)}$ [3], where A is the free parameter that is obtained while fitting. The spectrum shaping factor is obtained as -0.148 ± 0.007 and has a very good agreement between the value obtained using the dual monitor method and the value obtained by fitting the unfolded spectrum. The goodness of the fit or the R^2 value obtained is 0.93. Considering the improved accuracy that can be excepted when multiple monitors are used, the value -0.148 ± 0.007 is used in the further calculations.

3.2 Estimation of self-shielding factors

Neutron flux depression/fall experienced due to the sample presence is known as neutron self-shielding and it is important for isotopes with larger thermal absorption cross-sections or resonance integrals. Neutron cross-section measurements in a low flux facility requires samples with a weight of few grams compared to the milligram samples used in reactor experiments. In this scenario, the neutron self-shielding effect is of concern and the accuracy of cross-section measurements demands the estimation of self-shielding factors also. It can be estimated from the ratio of the reaction rate produced in the sample to the reaction rate produced in an infinitely diluted sample. The self-shielding correction factors in the thermal (G_{th}) and epithermal (G_{epi}) energies can be estimated analytically using the equations given below [7, 52, 53]

$$G_{th} = \frac{1-e^{-\xi}}{\xi} ; \qquad \xi = \frac{2}{\sqrt{\pi}} \frac{\rho N_A}{M} \sigma_0 t, \quad (6)$$

where t is the thickness of the target along the beam direction and ρ is the density of the target:

$$G_{epi} = \frac{0.94}{1 + (\frac{z}{2.70})^{0.82}} ; \qquad z = \frac{\rho N_A}{M} \sigma(E_{res}) 1.5 t \frac{\Gamma_\gamma}{\Gamma} , \quad (7)$$

Table 2. Thermal self-shielding correction factors (G_{th}) and epithermal self shielding correction factors (G_{epi}) of the samples under study estimated using Monte Carlo method and analytical formula.

	Monte Carlo method		Analytical method	
Foil	G_{th}	G_{epi}	G_{th}	G_{epi}
^{197}Au	0.97 ± 0.01	0.27 ± 0.01	0.98	0.27
^{55}Mn	0.99 ± 0.01	0.89 ± 0.02	0.99	0.89
^{139}La	0.99 ± 0.01	0.78 ± 0.02	0.99	0.80
^{140}Ce	0.99 ± 0.01	1.00 ± 0.01	0.99	0.99

Table 3. Relative uncertainties (%) of various parameters that contribute to the total uncertainty of the thermal capture cross-section estimation.

Sources of uncertainty	^{55}Mn	^{197}Au	^{139}La	^{140}Ce
Counting statistics (ΔC)	3.33	0.6	0.7	2.1
Half-life ($\Delta T_{1/2}$)	0.02	0.03	0.01	0.03
Gamma emission probability (ΔI_γ)	0.03	0.07	0.08	0.39
Detector dead time	0.1	0.1	0.1	0.1
Detector efficiency ($\Delta\epsilon$)	0.93	1.85	0.93	0.3
Sample mass (Δm)	0.5	0.5	0.2	0.2
Isotopic abundance ($\Delta\theta$)	–	–	0.007	0.057
Monitor cross-section ($\Delta\sigma_{0,Rf}$)	0.37	0.09	–	–
Self-shielding correction factor (ΔG_{th})	1.01	1.03	1.01	1.01
Total uncertainty	3.66	2.26	1.56	2.40

Table 4. Relative uncertainties (%) of various parameters that contribute to the total uncertainty in the resonance integral estimation. Reference monitors are also indicated in the table header next to the sample isotope.

Sources of uncertainty	^{139}La/^{55}Mn	^{139}La/^{197}Au	^{140}Ce/^{55}Mn	^{140}Ce/^{197}Au
Thermal self-shielding correction factor of reference ($\Delta G_{th,Rf}$)	0.88	0.91	0.75	0.77
Thermal self-shielding correction factor of sample ($\Delta G_{th,S}$)	0.89	0.90	0.76	0.76
Epithermal self-shielding correction factor of reference ($\Delta G_{epi,Rf}$)	1.99	3.30	1.68	2.80
Epithermal self-shielding correction factor of sample ($\Delta G_{epi,S}$)	2.21	2.23	0.74	0.75
Thermal capture cross-section of reference ($\Delta\sigma_{0,Rf}$)	0.42	0.08	0.36	0.07
Thermal capture cross-section of sample ($\Delta\sigma_{0,S}$)	3.72	2.34	4.17	3.00
Resonance integral of reference ($\Delta I_{0,Rf}$)	4.89	1.60	4.14	1.36
Effective resonance energy of reference ($\Delta E_{r,Rf}$)	0.91	0.88	0.77	0.75
Effective resonance energy of sample ($\Delta E_{r,S}$)	0.35	0.37	1.47	1.5
α-shaping parameter ($\Delta\alpha$)	0.73	1.34	1.53	3.26
Cadmium cut-off energy (ΔE_{Cd})	0.05	0.27	0.14	0.14
Cadmium ratio of reference ($\Delta F_{Cd,Rf}$)	3.67	0.99	3.13	0.87
Cadmium ratio of sample ($\Delta F_{Cd,S}$)	0.77	0.78	2.33	2.35
Total uncertainty	8.00	5.47	7.71	6.34

where $\sigma(E_{res})$ is the cross-section at the resonance peak corresponding to the energy E_{res}, Γ_γ is the resonance width corresponding to the neutron capture and Γ is the total resonance width. These values can be taken from the evaluated data file [29]. It can be seen that the self-shielding correction factors estimated analytically are universal and independent of the irradiation channel surroundings. The theoretical values depend on the macroscopic cross-sections, resonance widths and the thickness of the sample.

In addition, the self-shielding factors for the present experimental facility are estimated using a Monte Carlo method and compared with the values calculated analytically [54]. In the present work, the normalised spatial and energy distribution of the neutron flux over the three sides of the irradiation channel is used as the incident neutron source [3]. The exact dimension and material properties of the targets are used in the study. Reaction rates within the thermal and epithermal energy ranges are estimated using the combination of track length estimator and perturbation tally. The entire simulation is repeated for a sample with reduced density of 0.001 g/cm^3. The thermal and epithermal self-shielding factors are estimated from the ratios of reaction rates of the normal sample to the diluted sample of corresponding energy ranges. The self-shielding factors estimated using the Monte Carlo method and the analytical method are compared in table 2. It is found that generally both the methods agree within the uncertainty.

4 Measured thermal capture cross-sections and resonance integrals —results and discussions

It is important to provide well-documented uncertainty data along with the results since without the uncertainty information, the data may have no impact on the update of nuclear data [55]. The experimental uncertainties considered in thermal capture cross-section and resonance integral measurements are listed in table 3 and table 4. The uncertainties in the thermal cross-section estimation are between 2% and 5% and the total uncertainties in the resonance integral are between 5.5% and 8%, respectively. In the resonance integral estimation as shown in eq. (3) and eq. (4), various parameters are related nonlinearly. Hence, the uncertainties in each of these parameters are multiplied by respective error propagation factors to account this non-linear dependence [42, 50]. Most of the earlier measurement does not have the details about the uncertainty analysis or only statistical uncertainties are reported. Recent measurements are reported with total uncertainties considering the various parameters and it is important to note that the uncertainties of the present measurements are comparable with those measurements where reactor neutrons are used for irradiation [7, 36].

4.1 ^{139}La(n, γ)^{140}La

The thermal-neutron capture cross-section and resonance integrals of ^{139}La(n, γ)^{140}La estimated from the present measurements are compared with other literature values and listed in table 5. The plots of the cross-sections and the resonance integrals listed in table 5 are plotted as a function of the year of publication in fig. 3 and fig. 4, respectively. Since, most of the evalautions are in good agreement with each other only the ENDF/B-VII.1 [29] and the recommended data by Mughabghab [34] are included in the plot. The resonance integral listed from various evaluations are taken from table X of the compilation by Pritychenko and Mughabghab [35]. The presently measured σ_0 are 9.24 ± 0.25 b and 9.28 ± 0.37 b with reference to ^{197}Au and ^{55}Mn, respectively. Similarly, the measured resonance integral with respect to ^{197}Au is 12.18 ± 0.67 b

Table 5. Comparison of thermal neutron capture cross-section and resonance integral of ^{139}La(n, γ)^{140}La obtained from the present study with other measurements and evaluations. The type of EXFOR compilations in the case of thermal neutron capture cross sections is also indicated as MXW (Maxwellian average), SPA (Spectrum Average) and SIG (2200 m/s point cross-section).

Reference	σ_0 (b)	I_0 (b)	Incident spectra/neutron source	Type of σ_0 compilation
Present work	9.24 ± 0.25	12.18 ± 0.67	Modified Am-Be neutron spectra	SIG
Present work	9.28 ± 0.37	11.81 ± 0.94	Modified Am-Be neutron spectra	SIG
V.D. Nguyen *et al.*, 2014 [7]	9.16 ± 0.36	11.64 ± 0.69	Ta(γ, n) photonuclear reaction spectrum	SIG
F. Farina *et al.*, 2013 [8]	9.25 ± 0.04	–	Reactor spectrum	SIG
R. Terlizzi *et al.*, 2007 [19]	–	10.8 ± 1	(p, n) reaction spectrum from accelerator	TOF method
M. Takiue *et al.*, 1978 [9]	8.63 ± 0.34	–	Reactor spectrum	MXW
R.E. Heft, 1975 [20]	–	12.6 ± 0.6	Reactor spectrum	
W. Mannhart, 1975 [10]	8.933 ± 0.036	–	Reactor spectrum	SIG
E. Steinnes, 1975 [21]	–	11.2 ± 0.5	Reactor spectrum	
G. Gleason, 1975 [11]	9.15 ± 0.25	12.5 ± 0.4	Graphite moderated ^{252}Cf spectrum	MXW
Van Der Linden, 1974 [22]	–	11.6 ± 0.7	Reactor spectrum	
A. Alian *et al.*, 1973 [23]	–	17.1	Reactor spectrum	
E. Steinnes, 1972 [24]	–	11.8 ± 1.2	Reactor spectrum	
T.B. Ryves *et al.*, 1971 [25]	9.03 ± 0.33	7.5 ± 0.8	Deutron-beryllium reaction spectrum	SIG
E. Orvini *et al.*, 1968 [26]	–	10.8 ± 1.1	Reactor spectrum	
L. Breitenhuber *et al.*, 1968 [27]	–	11 ± 0.55	Reactor spectrum	
H.A. O'brien, 1967 [12]	9.5 ± 0.5	11.2 ± 0.6	Reactor spectrum	SIG
K.F. Alexander, 1964 [28]	–	12 ± 1	Reactor spectrum	
W.S. Lyon, 1960 [13]	8.1 ± 0.81	–	Reactor spectrum	SPA
J.D. Cummins, 1957 [14]	9.1 ± 0.2	–	Pile oscillator reactor spectrum	MXW
P. Benoist *et al.*, 1951 [15]	8.35 ± 0.1	–	Pile oscillator reactor spectrum	SIG
H. Pomerance, 1951 [16]	8.8 ± 0.44	–	Pile oscillator reactor spectrum	MXW
S.P. Harris *et al.*, 1950 [17]	9.01 ± 0.4505	–	Pile oscillator reactor spectrum	SPA
L. Seren *et al.*, 1947 [18]	8.4 ± 1.68	–	Reactor spectrum	SPA
Evaluations				
ENDF/B-VII.1 [29]	9.04	11.45		
JEFF 3.2 [30]	9.04	11.45		
JENDL 4.0 [5]	8.94	11.61		
ROSFOND-2010 [31]	9.04	11.45		
CENDL 3.1 [32]	9.04	11.45		
EAF-2010 [33]	8.94	11.95		
Mughabghab-2006 [34]	9.04 ± 0.04	12.1 ± 0.6		

and, with respect to ^{55}Mn, it is 11.81 ± 0.94 b. A very good agreement within the uncertainty is seen in the present measurements using two different reference monitors. Comparing with earlier measurements, the maximum deviations observed in the thermal capture cross-section now measured are 12.33% and 12.7% from the value (8.1 ± 0.81) reported by Lyon [13] which may be considered as an early measurement. The differences between the present measurements and the literature values after year 1960 are between 0.1% and 6.6% with ^{197}Au reference monitor estimation and between 0.3% and 7% with ^{55}Mn reference monitor estimation. When the Westcott factor is very close to unity (0.9996) as is the case of here for ^{139}La, the Maxwellian average cross-section is equivalent to the cross-section at 0.0253 eV. Resonance integral measurements are available only from year 1964. The differences between the present measurement and the other measured values in the case of the resonance integral are mostly between 1.4% and 11.3% with respect to ^{197}Au reference monitor and 1.4%–8.6% with respect to ^{55}Mn monitor except in case of the resonance integral reported by Ryves [25] and Alian *et al.* [23] (7.5 b and 17.1 b) where the differences are between 36% and 45%. It can be seen that the above two values are different from all other

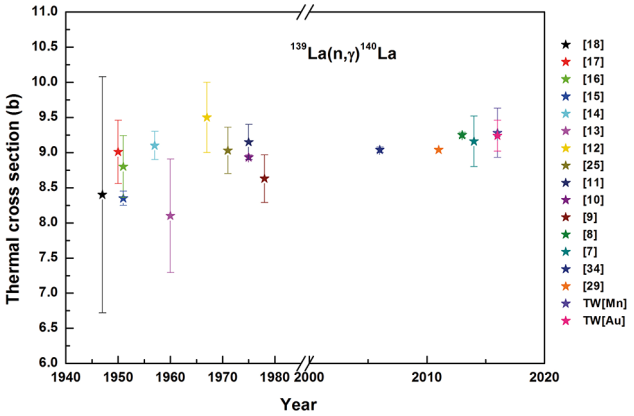

Fig. 3. The present measurements (represented by TW) of thermal capture cross-sections of ^{139}La compared with various literature values.

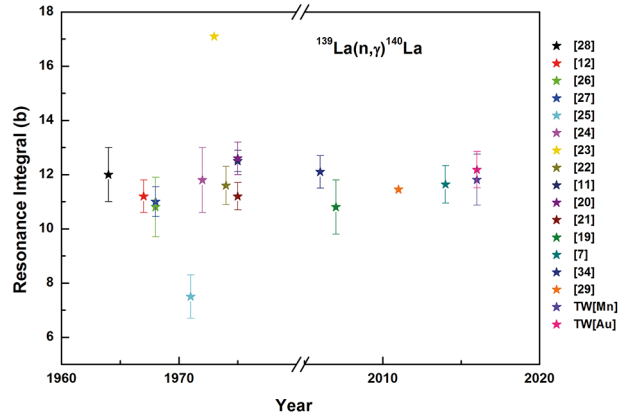

Fig. 4. The present measurements (represented by TW) of resonance integrals of ^{139}La compared with various literature values.

reported values and forms the upper and lower limit of the existing data having a spread of 9.6 b. The difference between various evaluations and the present measurements are between 2.1%–3.6% and 1.2%–6% for thermal capture cross-sections and resonance integrals, respectively. In short, deviations between the present measurements and various evaluations are nearly within the uncertainty in these measurements. On the whole, the present measurements confirm the established values of σ_0 and I_0 of ^{139}La(n, γ)^{140}La reaction and also the methodology followed in the present work.

4.2 ^{140}Ce(n, γ)^{141}Ce

The thermal-neutron capture cross-section and resonance integrals of ^{140}Ce(n, γ)^{141}Ce estimated from the present measurements are compared with other literature values and listed in table 6. The plots of the cross-sections and the resonance integrals listed in table 6 are plotted as a function of the year of publication in fig. 5 and fig. 6, respectively.

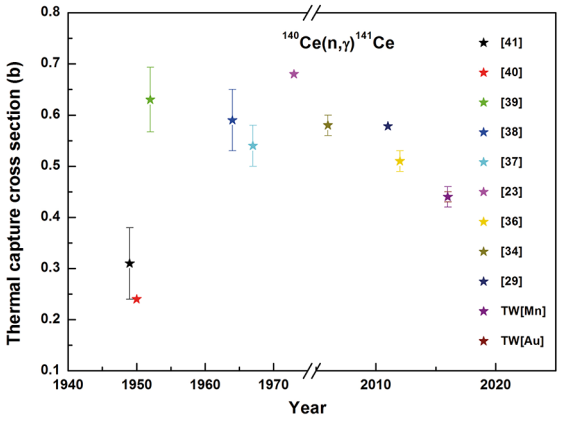

Fig. 5. The present measurements (represented by TW) of thermal capture cross sections of ^{140}Ce compared with various literature values.

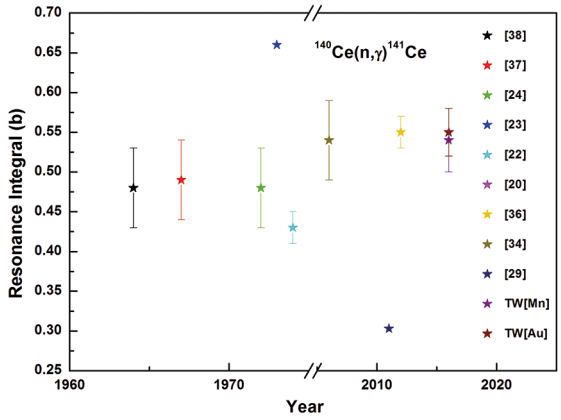

Fig. 6. The present measurements (represented by TW) of resonance integrals of ^{140}Ce compared with various literature values.

There is good agreement between the resonance integral and thermal capture cross-section measured with respect to ^{197}Au and ^{55}Mn reference monitor in the present measurements. The thermal capture cross-section value, which is small (0.44 ± 0.01 b and 0.44 ± 0.02 b), measured now is less uncertain than in the earlier measurements. The differences are between 15% and 54% or the maximum difference in the cross-section is only 0.24 b. When the Westcott factor is very close to unity (1.0003) as is the case here for ^{140}Ce, the Maxwellian average cross-section is equivalent to the cross-section at 0.0253 eV. The deviation between the present measurement and the recent measurement reported by Torrel and Krane is 15% or 0.07 b [36]. Thus, the measured values have not converged to a sufficient accuracy and also show a difference from the evaluations which are all nearly the same (0.58 b). The present measurements fulfill the need for more accurate measurements. The resonance integral measured in the present study (0.55 ± 0.03 b and 0.54 ± 0.04 b) are in good agreement with the recent measurement of Torrel and Krane (0–1.8% deviation) and the agreement between other measurements are between 10% and 22% in the case

Table 6. Comparison of thermal neutron capture cross-section and resonance integral of ^{140}Ce(n, γ)^{141}Ce obtained from the present study with other measurements and evaluations. The type of EXFOR compilations in the case of thermal neutron capture cross sections is also indicated as MXW (Maxwellian average) and SIG (2200 m/s point cross-section).

Reference	σ_0 (b)	I_0 (b)	Incident spectra/neutron source	Type of σ_0 compilation
Present work	0.44 ± 0.01	0.55 ± 0.03	Modified Am-Be neutron spectra	SIG
Present work	0.44 ± 0.02	0.54 ± 0.04	Modified Am-Be neutron spectra	SIG
S. Torrel *et al.*, 2012 [36]	0.51 ± 0.02	0.55 ± 0.02	Reactor spectrum	MXW
R.E. Heft, 1978 [20]	–	0.483 ± 0.005	Reactor spectrum	
Van Der Linden, 1974 [22]	–	0.43 ± 0.02	Reactor spectrum	
A. Alian *et al.*, 1973 [23]	0.68	0.66	Reactor spectrum	SIG
E. Steinnes, 1972 [24]	–	0.48 ± 0.05	Reactor spectrum	
J. Alstad *et al.*, 1967 [37]	0.54 ± 0.04	0.49 ± 0.05	Reactor spectrum	MXW
P.M. Lantz *et al.*, 1964 [38]	0.59 ± 0.06	0.48 ± 0.05	Reactor spectrum	MXW
H. Pomerance, 1952 [39]	0.63 ± 0.063	–	Pile oscillator thermal spectrum	MXW
D.J. Hughes *et al.*, 1950 [40]	0.24	–	Reactor spectrum	MXW
S. Katcoff *et al.*, 1949 [41]	0.31 ± 0.07	–	Reactor spectrum	MXW
Evaluations				
ENDF/B-VII.1 [29]	0.58	0.303		
JEFF 3.2 [30]	0.57	0.3366		
JENDL 4.0 [5]	0.57	0.345		
ROSFOND-2010 [31]	0.58	0.303		
CENDL 3.1 [32]	0.57	0.2801		
EAF-2010 [33]	0.58	0.2936		
Mughabghab-2006 [34]	0.58 ± 0.02	0.54 ± 0.05		

of ^{197}Au reference monitor and between 9% and 22% in the case of ^{55}Mn reference monitor. Most of the other reported measurements [22–24, 26, 38–40], except that of Alian *et al.* [23] are lower than the presently reported values. Interestingly the present measured resonance integral is in very good agreement with the evaluated resonance integral by Mughabghab [34]. However, all the other evaluations are lower than the presently measured values (from 36% to 49%) and also than the earlier measured values. It is clear that the resonance integral of ^{140}Ce(n, γ)^{141}Ce reaction which is not accurately known points to the need for revising the evaluations.

5 Summary

The thermal cross-sections and the resonance integrals for ^{139}La(n, γ)^{140}La and ^{140}Ce(n, γ)^{141}Ce are measured using an isotopic Am-Be source. The measured thermal cross-sections for ^{139}La are 9.24 ± 0.25 b and 9.28 ± 0.37 with reference to ^{197}Au and ^{55}Mn, respectively. The resonance integral for ^{139}La with respect to ^{197}Au reference is 12.18 ± 0.67 b and with respect to ^{55}Mn is 11.81 ± 0.94 b. The measured thermal cross-section for ^{140}Ce with respect to ^{197}Au reference is 0.44 ± 0.01 and with respect to b ^{55}Mn reference is 0.44 ± 0.02 b. The resonance integral for ^{140}Ce with respect to ^{197}Au is 0.55 ± 0.03 b and with respect to ^{55}Mn is 0.54 ± 0.04 b. The following conclusions can be made from the present measurements and their comparisons with existing data.

- The present results confirm the cross-section evaluations as well as earlier measurements for ^{139}La(n, γ) ^{140}La reaction.
- For the ^{140}Ce(n, γ)^{141}Ce reaction, the presently measured thermal cross-section and resonance integral values do not agree with earlier measured data which have large scatter among themselves. The present thermal cross-section values underpredict the evaluated data and the resonance integral values match with the other recent measurement, but are higher than the evaluations requiring more accurate measurements.

Based on the present study, the following observations are made about the methodology followed in the estimation of the self-shielding correction factors and epithermal spectrum shaping factor as well as about the reference monitors used.

- The results obtained from the present study with respect to ^{197}Au and ^{55}Mn show a very good agreement with each other. The Westcott factor and the effective resonance energy of ^{197}Au and ^{55}Mn are very different. The incorporation of both these sets of values in the estimation of thermal caprure cross-section and resonance integral makes the measured values independent of the reference monitor selected. However, due to the lower counting statistics of ^{55}Mn, the uncertainty in the thermal capture cross-sections and the resonance integrals measured with reference to ^{55}Mn monitor is slightly greater than that measured with reference to the ^{197}Au monitor.

– The accurate estimation of epithermal self-shielding factor is important for the resonance integral measurement using larger samples needed for the activation in a low flux facility like the Am-Be source. Monte Carlo method results which were compared with those of the analytical method here are expected to give a higher accuracy of the measurement results for such samples.
– The epithermal spectrum shaping factor is estimated in the present study using two different methods: i) fitting of unfolded spectra obtained from multiple foil activation and ii) dual monitor comparison method. A good agreement is seen between the two estimations. But the more elaborate former approach is to be preferred for a higher accuracy of the measurement results.

The financial support provided by Manipal Centre for Natural Sciences (MCNS), Manipal University is acknowledged. The first author acknowledges the research grant (YSS/2015/000899) from Science and Engineering Research Board (SERB), India. The authors are thankful to Dr. V. Gopalakrishnan, MCNS for generating the activation cross-sections of the Mo isotope used for multi-foil irradiation to determine the neutron spectrum.

References

1. M. Barbagallo, N. Colonna, S. Altstadt, J. Andrzejewski, L. Audouin, V. Bécares, F. Bečvář, F. Belloni, E. Berthoumieux, J. Billowes *et al.*, EPJ Web of Conferences **66**, 10001 (2014).
2. S. Ganesan, Nucl. Data Sheets **123**, 21 (2015).
3. P. Panikkath, P. Mohanakrishnan, Eur. Phys. J. A **52**, 276 (2016).
4. L. Danu, P. Joshi, D. Biswas, S. Mukhopadhyay, A. Goswami, P. Prashanth, L. Kinage, R. Choudhury, B. Singh, Eur. Phys. J. A **48**, 1 (2012).
5. K. Shibata, O. Iwamoto, T. Nakagawa, N. Iwamoto, A. Ichihara, S. Kunieda, S. Chiba, K. Furutaka, N. Otuka, T. Ohasawa *et al.*, J. Nucl. Sci. Technol. **48**, 1 (2011).
6. N. Otuka, E. Dupont, V. Semkova, B. Pritychenko, A. Blokhin, M. Aikawa, S. Babykina, M. Bossant, G. Chen, S. Dunaeva *et al.*, Nucl. Data Sheets **120**, 272 (2014).
7. N. Van Do, P.D. Khue, K.T. Thanh, N.T. Hien, G. Kim, S. Yang, Y.S. Cho, T.Y. Song, Y.O. Lee, S.G. Shin *et al.*, Nucl. Instrum. Methods Phys. Res. B **335**, 1 (2014).
8. F. Farina, P. Vermaercke, K. Smits, L. Sneyers, K. Strijckmans, J. Radioanal. Nucl. Chem. **296**, 931 (2013).
9. M. Takiue, H. Ishikawa, Nucl. Instrum. Methods **148**, 157 (1978).
10. W. Mannhart, Tech. Rep., Technische Univ. Muenchen, Garching (FR Germany), Physik-Department (1975).
11. G. Gleason, Radiochem. Radioanal. Lett. **23**, 317 (1975).
12. H. O'Brien, J. Eldridge, R. Druschel, J. Halperin, J. Inorg. Nucl. Chem. **29**, 584 (1967).
13. W. Lyon, Nucl. Sci. Eng. **8**, 378 (1960).
14. J. Cummins, Tech. Rep., United Kingdom Atomic Energy Authority. Research Group, Atomic Energy Research Establishment, Harwell, Berks, England (1957).
15. P. Benoist, L. Kowarski, F. Netter, J. Phys. Radium (Paris) **12**, 584 (1951).
16. H. Pomerance, Phys. Rev. **83**, 641 (1951).
17. S. Harris, C.O. Muehlhause, G. Thomas, Phys. Rev. **79**, 11 (1950).
18. L. Seren, H.N. Friedlander, S.H. Turkel, Phys. Rev. **72**, 888 (1947).
19. R. Terlizzi, U. Abbondanno, G. Aerts, H. Alvarez, F. Alvarez-Velarde, S. Andriamonje, J. Andrzejewski, P. Assimakopoulos, L. Audouin, G. Badurek *et al.*, Phys. Rev. C **75**, 035807 (2007).
20. R. Heft, *A consistent set of nuclear-parameter values for absolute instrumental neutron activation analysis*, in *Proceedings of the American Nuclear Society Topical Conference on Computers in Activation Analysis and Gamma-Ray Spectroscopy, Mayaguez, Puerto Rico, 1978* (National Technical Information Service, U.S. Dept. of Commerce, 1979) p. 495.
21. E. Steinnes, J. Inorg. Nucl. Chem. **37**, 1591 (1975).
22. R. Van der Linden, F. De Corte, J. Hoste, J. Radioanal. Chem. **20**, 695 (1974).
23. A. Alian, H. Born, J. Kim, J. Radioanal. Nucl. Chem. **15**, 535 (1973).
24. E. Steinnes, J. Inorg. Nucl. Chem. **34**, 2699 (1972).
25. T. Ryves, J. Nucl. Energy **25**, 129 (1971).
26. E. Orvini, G. Gaggero, L. Lesca, A. Bresesti, M. Bresesti, J. Inorg. Nucl. Chem. **30**, 1353 (1968).
27. L. Breitenhuber, M. Pinter, Progress Report 68 (IAEA, 1968), report from misc. OECD Countries to EANDC.
28. K.F. Alexander, Tech. Rep. 23 (1964) zentralinst. f. Kernforschung Rossendorf Reports.
29. M. Chadwick, M. Herman, P. Obložinskỳ, M.E. Dunn, Y. Danon, A. Kahler, D.L. Smith, B. Pritychenko, G. Arbanas, R. Arcilla *et al.*, Nucl. Data Sheets **112**, 2887 (2011).
30. A. Koning, E. Bauge, C. Dean, E. Dupont, U. Fischer, R. Forrest, R. Jacqmin, H. Leeb, M. Kellett, R. Mills *et al.*, J. Korean Phys. Soc. **59**, 1057 (2011).
31. S. Zabrodskaya, A. Ignatyuk, V. Koscheev *et al.*, *RUSFOND - Russian National Library of Evaluated Neutron Data*, in *VANT, Problems of Atomic Science and Technology - Series: Nuclear and Reactor Constants*, issue no. 1-2 (2007) pp. 3–21.
32. Z. Ge, Z. Zhao, H. Xia, Y. Zhuang, T. Liu, J. Zhang, H. Wu, J. Korean Phys. Soc. **59**, 1052 (2011).
33. J.C. Sublet, L. Packer, J. Kopecky, R. Forrest, A. Koning, D. Rochman, CCFE Report, CCFE R(10)05 (2010).
34. S.F. Mughabghab, *Atlas of Neutron Resonances: Resonance Parameters and Thermal Cross Sections. Z* = 1–100 (Elsevier, 2006).
35. B. Pritychenko, S. Mughabghab, Nucl. Data Sheets **113**, 3120 (2012).
36. S. Torrel, K. Krane, Phys. Rev. C **86**, 034340 (2012).
37. J. Alstad, T. Jahnsen, A. Pappas, J. Inorg. Nucl. Chem. **29**, 2155 (1967).
38. P. Lantz, C. Baldock, L. Idom, Nucl. Sci. Eng. **20**, 302 (1964).
39. H. Pomerance, Phys. Rev. **88**, 412 (1952).
40. D. Hughes, D. Sherman, Phys. Rev. **78**, 632 (1950).
41. S. Katcoff, J. Leary, K. Walsh, R. Elmer, S. Goldsmith, L. Hall, E. Newbury, J. Povelites, J. Waddell, J. Chem. Phys. **17**, 421 (1949).
42. M. Karadag, H. Yücel, Nucl. Instrum. Methods Phys. Res. A **550**, 626 (2005).

43. W. McElroy, *A computer-automated iterative method for neutron flux spectra determination by foil activation*, Technical Report (U.S. Dept. of Defense, 1967).
44. IAEA, *Reference neutron activation library*, IAEA-TECDOC-1285 (International Atomic Energy Agenc, Vienna, 2002).
45. J.F. Briesmeister *et al.*, *MCNP –A general Monte Carlo code for neutron and photon transport* (Los Alamos National Laboratory, 1986).
46. B. Marie-Martine, Valery P. Chechev, Nucl. Instrum. Methods Phys. Res. A **728**, 157 (2013).
47. M. Berger, J. Hubbell, S. Seltzer, J. Chang, J. Coursey, R. Sukumar, D. Zucker, K. Olsen, *NIST Standard Reference Database* 8 (NIST, 1990).
48. F. De Corte, A. Simonits, A. De Wispelaere, J. Radioanal. Nucl. Chem. **133**, 131 (1989).
49. F. De Corte, K. Sordo-El Hammami, L. Moens, A. Simonits, A. De Wispelaere, J. Hoste, J. Radioanal. Chem. **62**, 209 (1981).
50. H. Yücel, M. Karadag, Ann. Nucl. Energy **31**, 681 (2004).
51. R.B.M. Sogbadji, B.J.B. Nyarko, E.H.K. Akaho, R.G. Abrefah, World J. Nucl. Sci. Technol. **1**, 50 (2011).
52. M. Blaauw, Nucl. Instrum. Methods Phys. Res. A **356**, 403 (1995).
53. E. Martinho, I. Gonçalves, J. Salgado, Appl. Radiat. Isot. **58**, 371 (2003).
54. A. Trkov, G. Žerovnik, L. Snoj, M. Ravnik, Nucl. Instrum. Methods Phys. Res. A **610**, 553 (2009).
55. D. Smith, N. Otuka, Nucl. Data Sheets **113**, 3006 (2012).